Influence of the lattice water molecules on magnetization dynamics of binuclear dysprosium(III) compounds: insights from magnetic and *ab initio* calculations

Jiyuan Du,‡[a] Shilong Wei,‡[b] Zhijie Jiang,[d] Hongshan Ke,[b] Lin Sun,*[a] Yiquan Zhang,*[c] Sanping Chen*[b]

a. Henan Key Laboratory of Polyoxometalate Chemistry, College of Chemistry and Chemical Engineering, Henan University, Kaifeng, Henan 475004, China

b. Key Laboratory of Synthetic and Natural Functional Molecule Chemistry of Ministry of Education, College of Chemistry and Materials Science, Northwest University, Xi'an, Shaanxi 710069, China.

c. Jiangsu Key Laboratory for NSLSCS, School of Physical Science and Technology, Nanjing Normal University, Nanjing 210023, China.

d. Shaanxi Xueqian Normal University, Xian, Shanxi, 710100, China.

‡These authors have equal contribution to this study.

* Corresponding author: Lin Sun, Yiquan Zhang, Sanping Chen

Email address: sunlin@vip.henu.edu.cn (L. Sun); zhangyiquan@njnu.edu.cn (Y.Q. Zhang); sanpingchen@126.com (S. P. Chen)

Contents

Graphs and Tables

susceptibility of **1** under 0 Oe dc field.

Figure S16. Temperature dependence of the in-phase (a) and out-of-phase (b) ac susceptibility of **2** under 0 Oe dc field.

Table S8. Relaxation fitting parameters from Least-Squares Fitting of $\chi(\omega)$ data of **1**.

Table S9. Relaxation fitting parameters from Least-Squares Fitting of $\chi(\omega)$ data of **2**.

Figure S17. Calculated complete structures for**1**and **2**; H atoms are omitted.

Table S10. Calculated energy levels (cm^{-1}) and $\boldsymbol{g}$ (g_x, g_y, g_z) tensors of the lowest Kramers doublets (KDs) of one Dy^{III} center of **1** and **2**.

Table S11. Exchange energies E (cm^{-1}) and the main values of the g_z for the lowest two exchange doublets of **1** and **2** *via* fitting the experimental $\chi_M T$ versus T (M versus H) by using POLY_ANISO program.

Table S12. The angle between the *ab initio* easy axis and angle between easy axis on Dy1 and Dy1-Dy2 of compounds **1** and **2.**

Table S13. The angle between the *ab initio* easy axis and the axial Dy-O/N bond of compounds **1** and **2.**

Table S14. Natural Bond Order (NBO) charges per atoms in the ground state of **1** and **2** calculated within CASSCF.

Table S15. The results of preliminary ESP (in a.u.) analysis of **1** and **2.**

Table S16. Wave functions with definite projection of the total moment $| m_J >$ for the lowest eight KDs of individual Dy^{III} fragments for **1** and **2**.

Table S17. Relaxation parameters and the value of U_{eff} for nine-coordinated Dy_2 compounds with C_{4v}-CSAPR geometries.

Figure S18. The relationship between coordination configuration and SMM behavior.

1.Materials and Instruction

All materials and reagents for the synthesis were commercially available and used without any further purification. FT-IR spectra were recorded in the range of 400–4000 cm^{-1} using KBr pellets on an EQUINOX55 FT/IR spectrophotometer and samples were prepared as KBr pellets. Elemental analysis for C, H and N was carried out a Perkin-Elmer 2400 CHN elemental analyzer. Powder X-ray diffraction (PXRD) measurements were executed on a Rigaku RU200 diffractometer at 60 kV, 300 mA with Cu Kα radiation as the radiation source (λ = 1.5406 Å) in the angular range θ =5-50° at 25 °C. Thermogravimetric analysis (TGA) was conducted on a NETZSCH TG 209 thermal analyzer in the atmosphere of nitrogen at a heating rate of 10 °C/min. The thermodynamic parameters were measured by a TA/Nano isothermal titration calorimeter. Magnetic measurements were performed in the temperature range 2 K - 300 K with an applied field of 1000 Oe, using a Quantum Design MPMS-XL-7 SQUID magnetometer on polycrystalline samples. The freshly prepared crystalline samples wrapped into a piece of parafilm and packed in a polyethylene bag was pelletized to avoid any field induced crystal reorientation. The diamagnetic corrections for compounds were estimated using Pascal's constants. Alternating current (ac) susceptibility experiments were performed using an oscillating ac field of 2.0 Oe at ac frequencies ranging from 1 to 1000 Hz. The magnetization was measured in the field range 0 - 7 T.

2. Thermogravimetric analysis

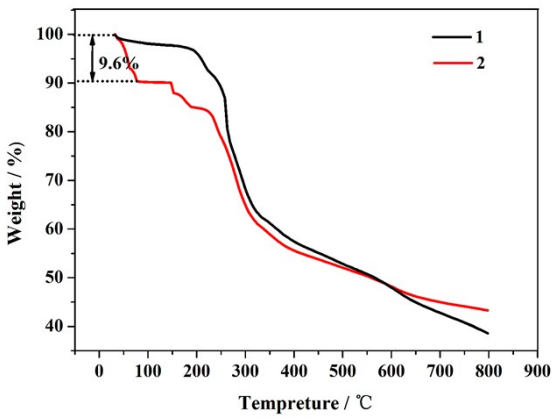

Figure S1. TGA of **1** and **2** under dry N_2 atmosphere.

3.X-Ray Powder Diffraction.

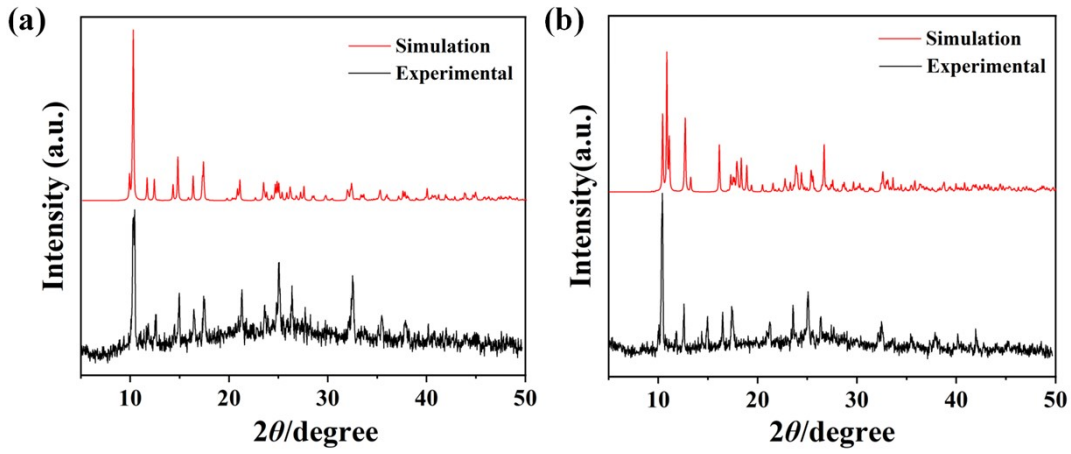

Figure S2. Experimental PXRD and calculated PXRD of **1**(a) and **2**(b).

4.X-ray Crystallography.

The single crystal X-ray experiment was employed using Rigaku SCX mini CCD diffractometer equipped with Mo Kα radiation(λ = 0.71073 Å radiation) and ω and φ scanning mode. The SAINT and the SADABS software were performed for absorption correction.[S5-S6] The structures of **1** and **2** were solved by the direct method and refined by full-matrix least-squares on F^2 using SHELXL-97 and SHELXL-2016 programs. [S7-S8] Anisotropic displacement parameters were employed for all non-hydrogen atoms. Hydrogen atoms were assigned to their calculated positions and subsequently allowed to ride on their parent atoms. CCDC-1553638 for **1** and CCDC-1553639 for **2** can be obtained via Cambridge Crystallographic Data clicking www.ccdc.cam.ac.uk/ data_request/cif.

Table S1. Crystallographic Data for**1** and **2**.

Compound	**1**	**2**
Empirical formula	$C_{30}H_{34}Dy_2N_{12}O_{12}$	$C_{30}H_{46}Dy_2N_{12}O_{18}$
Formula weight	1079.69	1187.79
Temperature	296(2) K	296(2) K
Crystal system	Monoclinic	Triclinic
space group	$P2_1/n$	P-1

a (Å)	11.302(2)	9.182(5)
b (Å)	14.387(3)	10.720(6)
c (Å)	11.454(2)	12.462(7)
α (°)	90	86.385(10)
β (°)	105.017(3)	88.762(9)
γ (°)	90	67.666(8)
V (Å^3)	1798.8(6)	1132.4(11)
Z	2	1
F(000)	1052	586
Goodness-of-fit on *F*^2	1.004	1.022
Final *R* indices [*I*>2sigma(*I*)]	*R*1 = 0.0396	*R*1 = 0.0614
R indices (all data)	*R*1 = 0.0682	*R*1 = 0.0960
CCDC	1553638	1553639

Table S2. Selected bond lengths (Å) and angles (°) for **1** and **2**.

1		**2**	
Dy(1)-O(3)	2.296(5)	Dy(1)-O(3)	2.299(6)
Dy(1)-O(6)	2.342(4)	Dy(1)-O(6)	2.324(8)
Dy(1)-O(7)	2.387(4)	Dy(1)-O(7)	2.346(7)
Dy(1)-N(2)	2.412(6)	Dy(1)-O(5)	2.396(8)
Dy(1)-O(2)	2.450(6)	Dy(1)-O(2)	2.411(8)
Dy(1)-O(4)	2.451(5)	Dy(1)-N(2)	2.420(9)
Dy(1)-O(1)	2.488(6)	Dy(1)-O(1)	2.422(8)
Dy(1)-N(1)	2.538(6)	Dy(1)-N(1)	2.581(8)
Dy(1)-O(5)	2.604(5)	Dy(1)-O(4)	2.582(7)
O(3)-Dy(1)-O(6)	75.09(16)	O(3)-Dy(1)-O(6)	82.8(3)
O(3)-Dy(1)-O(7)	145.79(16)	O(3)-Dy(1)-O(7)	145.1(2)
O(5)-Dy(1)-O(7)	78.52(16)	O(6)-Dy(1)-O(7)	74.0(3)
O(7)-Dy(1)-N(2)	64.67(18)	O(3)-Dy(1)-O(5)	85.2(3)
O(6)-Dy(1)-N(2)	87.01(18)	O(6)-Dy(1)-O(5)	118.4(2)
O(7)-Dy(1)-O(2)	121.29(18)	O(7)-Dy(1)-O(5)	83.4(3)
N(2)-Dy(1)-O(2)	77.18(19)	O(3)-Dy(1)-O(3)	81.1(3)
O(3)-Dy(1)-O(4)	95.69(17)	O(6)-Dy(1)-O(3)	158.0(3)
O(6)-Dy(1)-O(4)	118.22(16)	O(7)-Dy(1)-O(3)	126.9(3)
O(7)-Dy(1)-O(4)	78.01(17)	O(5)-Dy(1)-O(3)	75.2(3)
N(2)-Dy(1)-O(4)	75.86(18)	O(3)-Dy(1)-N(2)	64.5(3)
O(2)-Dy(1)-O(4)	152.17(17)	O(6)-Dy(1)-N(2)	84.4(3)

O(3)-Dy(1)-O(1)	125.36(19)	O(7)-Dy(1)-N(2)	136.1(3)
O(5)-Dy(1)-O(1)	82.27(19)	O(5)-Dy(1)-N(2)	140.2(3)
O(7)-Dy(1)-O(1)	71.07(18)	O(2)-Dy(1)-N(2)	75.2(3)
N(2)-Dy(1)-O(1)	113.6(2)	O(3)-Dy(1)-O(1)	133.8(3)
O(2)-Dy(1)-O(1)	50.59(18)	O(6)-Dy(1)-O(1)	143.1(3)
O(4)-Dy(1)-O(1)	138.48(19)	O(7)-Dy(1)-O(1)	74.8(3)
O(3)-Dy(1)-N(1)	128.45(18)	O(3)-Dy(1)-O(1)	76.6(3)
O(6)-Dy(1)-N(1)	154.68(19)	O(2)-Dy(1)-O(4)	53.3(3)
O(7)-Dy(1)-N(1)	82.33(18)	N(2)-Dy(1)-O(4)	105.4(3)
N(2)-Dy(1)-N(1)	63.8(2)	O(5)-Dy(1)-N(1)	125.6(3)
O(2)-Dy(1)-N(1)	88.94(19)	O(1)-Dy(1)-N(1)	81.9(3)
O(4)-Dy(1)-N(1)	73.05(17)	O(6)-Dy(1)-N(1)	77.0(3)
O(3)-Dy(1)-N(1)	75.9(2)	O(5)-Dy(1)-N(1)	146.6(3)
O(3)-Dy(1)-O(5)	77.98(16)	O(2)-Dy(1)-N(1)	95.3(3)
O(6)-Dy(1)-O(5)	67.62(17)	N(2)-Dy(1)-N(1)	62.2(3)
O(7)-Dy(1)-O(5)	72.03(15)	O(4)-Dy(1)-N(1)	72.3(3)
N(2)-Dy(1)-O(5)	110.17(17)	O(3)-Dy(1)-O(5)	71.8(2)
O(2)-Dy(1)-O(5)	149.20(17)	O(5)-Dy(1)-O(5)	67.6(3)
O(4)-Dy(1)-O(5)	50.89(14)	O(7)-Dy(1)-O(5)	75.4(2)
O(1)-Dy(1)-O(5)	136.01(18)	O(6)-Dy(1)-O(5)	51.3(2)
N(1)-Dy(1)-O(5)	121.46(17)	O(2)-Dy(1)-O(5)	120.6(3)
(i) 1-*x*, -*y*, 2-*z*.		(i) -*x*+1, -*y*+1, -*z*+1.	

5.Thermodynamics of the Reaction System of 1 and 2

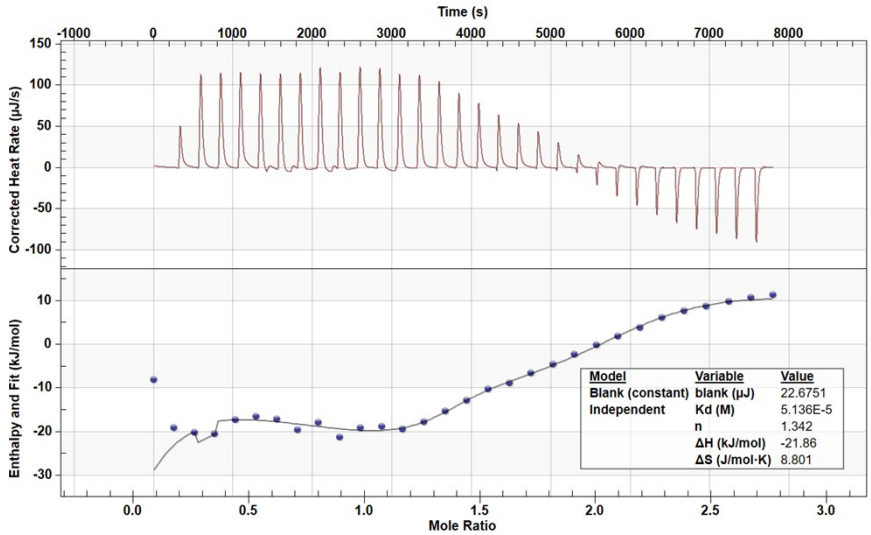

Figure S3. The titration curves at 298 K of the system of S-1.

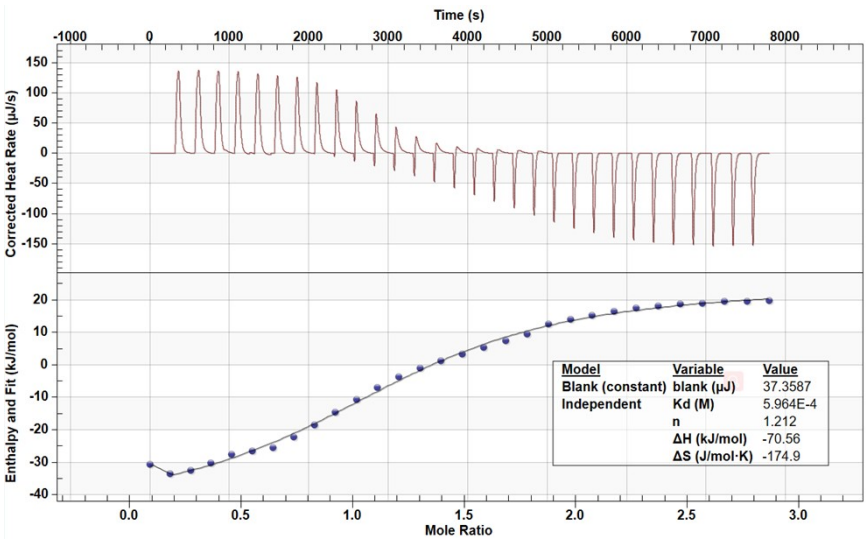

Figure S

Figure S4. The titration curves at 298 K of the system of S-2.

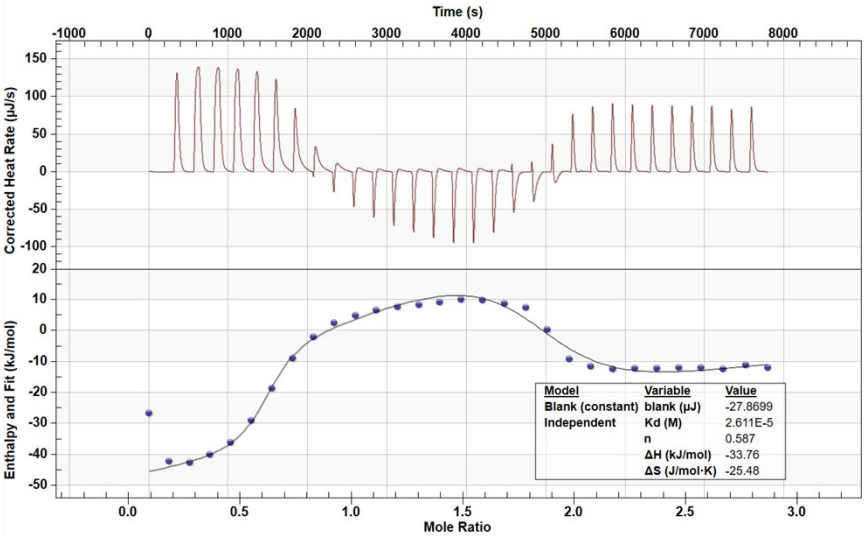

Figure S5. The titration curves at 298 K of the system of S-3.

6.Crystal Structure

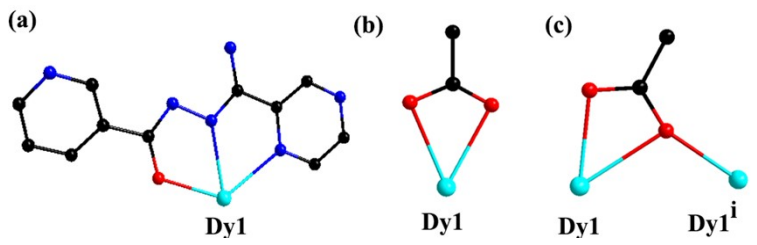

Figure S6. (a) Connection mode of 2,3′-Hppcad ligand and two coordinate modes of acetate groups: (b) η^2; (c)η^1:η^2:μ_2.

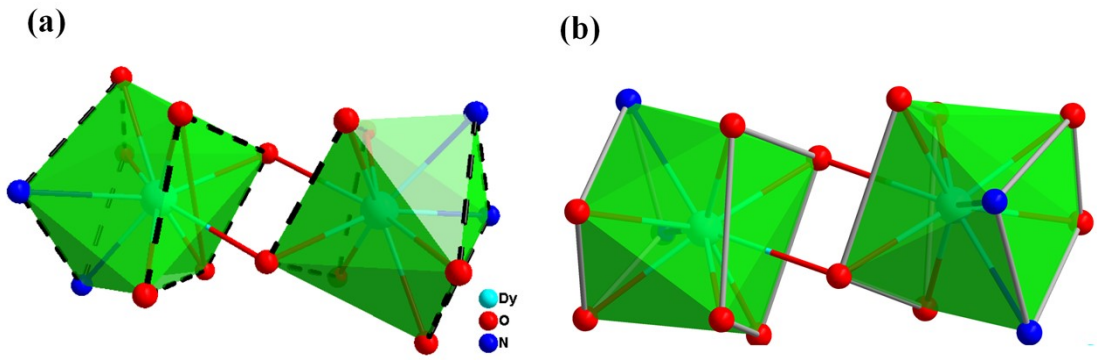

Figure S7. Local coordination geometry of the Dy^{III} ion in 1(a) and 2(b).

Table S3. The calculated results for Dy^{III} ions configuration of **1** and **2** by SHAPE 2.1 software.

Configuration	ABOXIY, **1**	ABOXIY, **2**
Octagonal pyramid (C_{8v})	23.069	23.824
Heptagonal bipyramid (D_{7h})	17.943	16.871
Johnson Triangular cupola J3 (C_{3v})	14.264	13.198
Capped Cube J8 (C_{4v})	9.759	8.934
Spherical-relaxed capped Cube (C_{4v})	8.623	8.445
Capped square antiprism J10 (C_{4v})	3.438	2.415
Spherical capped square antiprism (C_{4v})	**2.419**	**2.015**
Tricapped trigonal prism J51 (D_{3h})	3.816	3.599
Spherical tricapped trigonal prism (D_{3h})	3.029	2.774
Tridiminished icosahedron J63 (C_{3v})	10.556	11.339

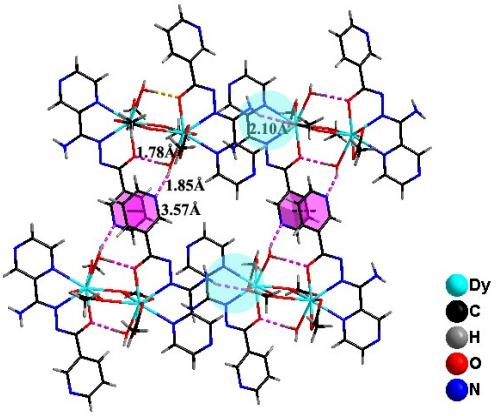

Figure S8. Packing diagram for compound **1**. The black dotted lines represent the $\pi\cdots\pi$ interactions, and the purple dotted lines represent the hydrogen bonding interactions.

Table S4. Hydrogen bond geometry in **1**.

D-H···A	$d_{D\text{-}H}$/Å	$\boldsymbol{d_{H\cdots A}}$/Å	$d_{D\cdots A}$/Å	∠ DHA°
O(6)-H(6B)···N(7)^{ii}	0.96	1.85	2.741(8)	153.5
O(6)-H(6A)···O(5)^{i}	0.96	1.78	2.738(7)	174.4
N(4)-H(4D)···O(4)^{iii}	0.89	2.10	2.945(8)	158.7

(i) 1-*x*, -*y*, 2-*z*; (ii) -1+*x*, *y*, *z*; (iii) 1-*x*, 1-*y*, 2-*z*.

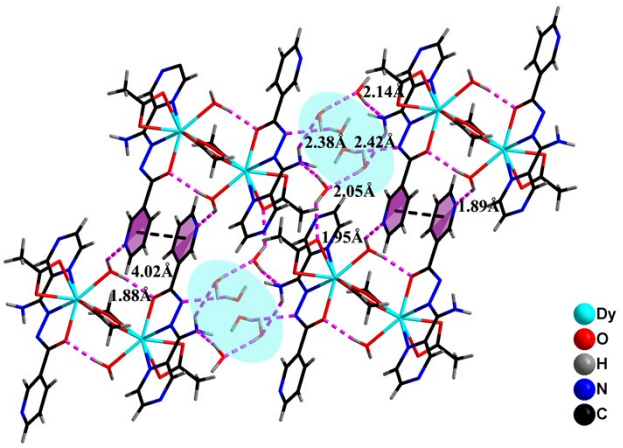

Figure S9. Packing diagram for 2. The black dotted lines represent the $\pi\cdots\pi$ interactions, and the purple dotted lines represent the hydrogen bonding interactions.

Table S5. Hydrogen bond geometry in **2**.

D-H···A	$d_{D\text{-}H}$/Å	$\boldsymbol{d_{H\cdots A}}$/Å	$d_{D\cdots A}$/Å	∠ DHA°
O(8A)-H(8AB)···O(4)	1.04	1.95	2.789(1)	135.5
O(8A)-H(8AA)···N(3)^{ii}	0.92	2.14	3.011(1)	157.3
O(9)-H(9B)···O(8A)	0.97	2.05	2.910(2)	146.9
O(8)-H(8B)···N(1)^{iii}	0.95	2.42	2.993(2)	118.9
N(3)-H(3B)···O(9)^{v}	0.80	2.38	3.050(2)	141.8
O(6)-H(6B)···O(5)^{i}	0.89	1.88	2.734(1)	160.3
O(6)-H(6A)···N(5)^{vi}	0.99	1.89	2.696(1)	136.8

(i) -*x*+1, -*y*+1, -*z*+1; (ii) -*x*+1, -*y*+1, -*z*; (iii) *x*, *y*-1, *z*; (iv) -*x*, -*y*+1, -*z*+1; (v) *x*-1, *y*+1, *z*; (vi) *x*+1, *y*-1, *z*.

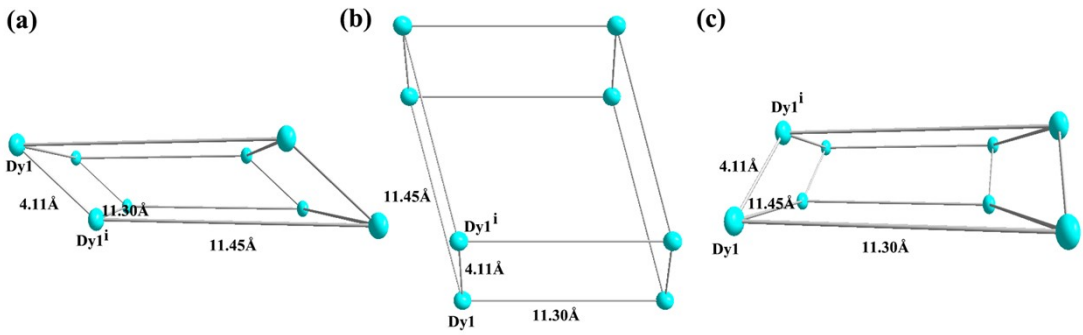

Figure S10. The distances of dinuclear Dy units in compound **1**. (a) along the *a* axis; (b) along the *b* axis; (c) along the *c* axis.

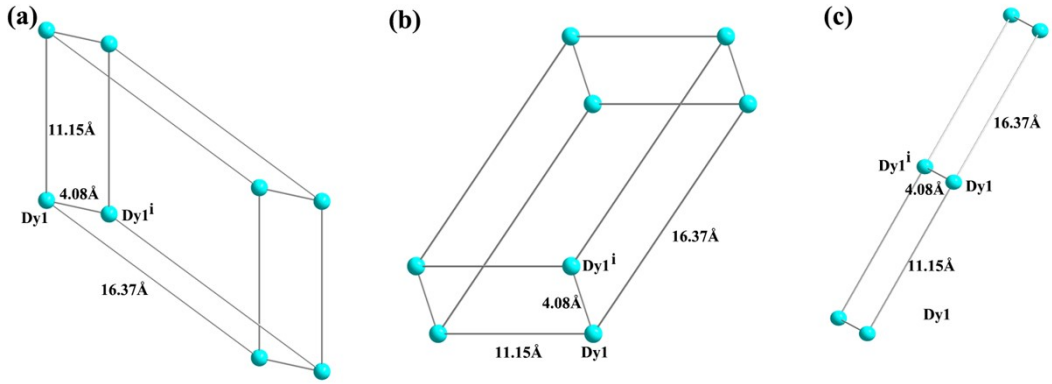

Figure S11. The distances of dinuclear Dy units in compound **2**. (a) along the *a* axis; (b) along the *b* axis; (c) along the *c* axis.

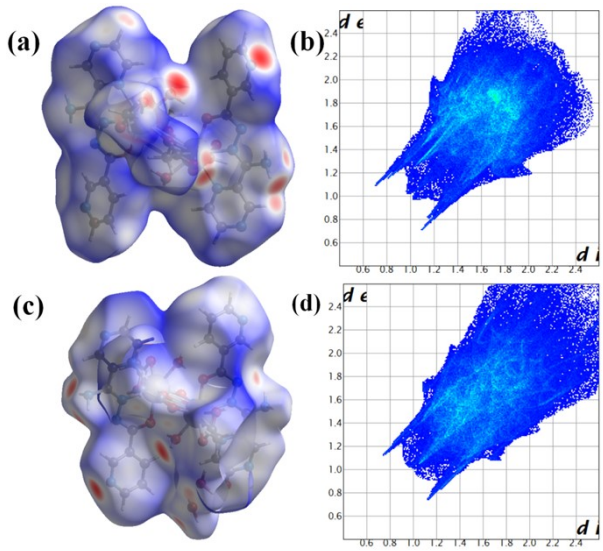

Figure S12. Hirshfeld surfaces calculation of **1**(a) and **2**(c) two-dimensional fingerprint plots in the crystal stacking of **1**(b) and **2**(d).

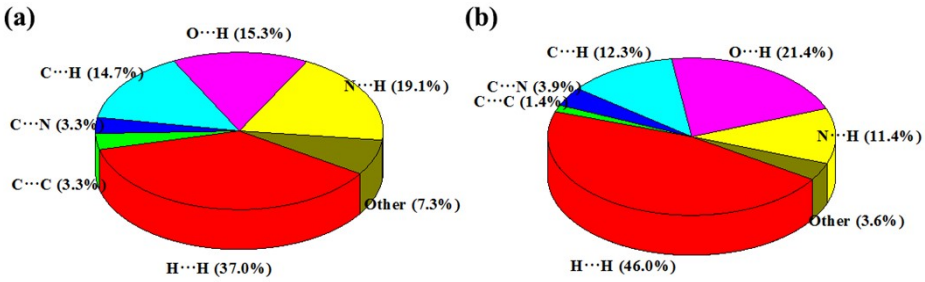

Figure S13. Individual atomic contact percentage contribution to the Hirshfeld surface for **1**(a) and **2**(c).

7.Magnetic Measurements

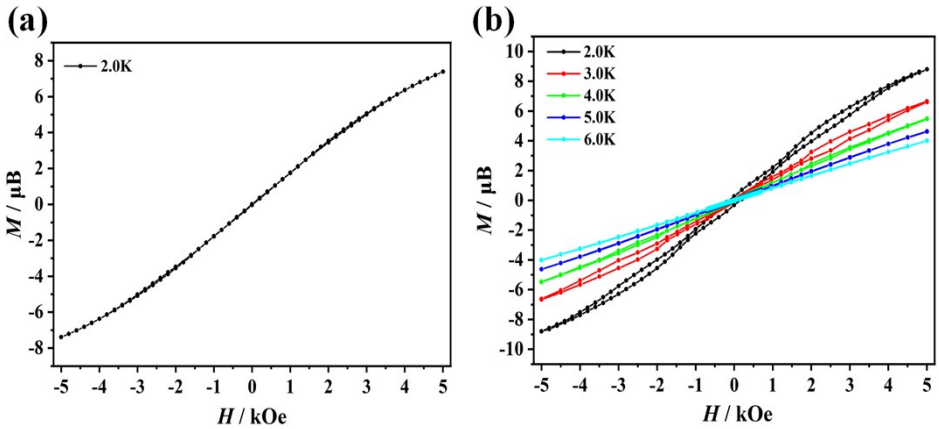

Figure S14. Magnetic hysteresis loops for **1** (a) and **2** (b)on a sweep rate of 100 Oe/min.

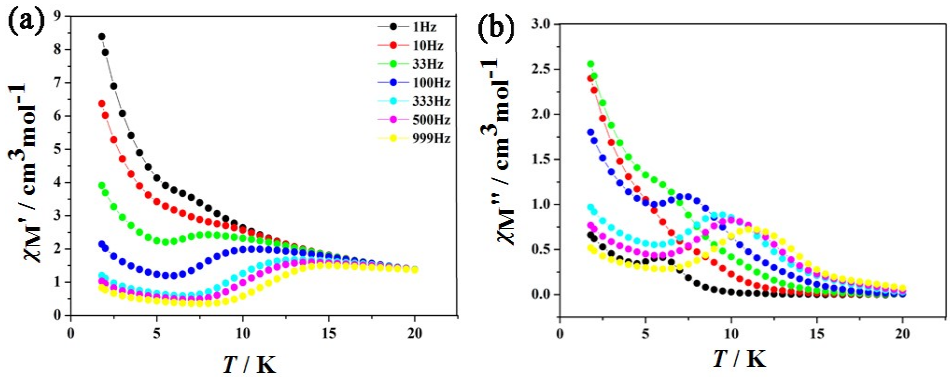

Figure S15. Temperature dependence of the in-phase (a) and out-of-phase (b) ac susceptibility of **1** under 0 Oe dc field.

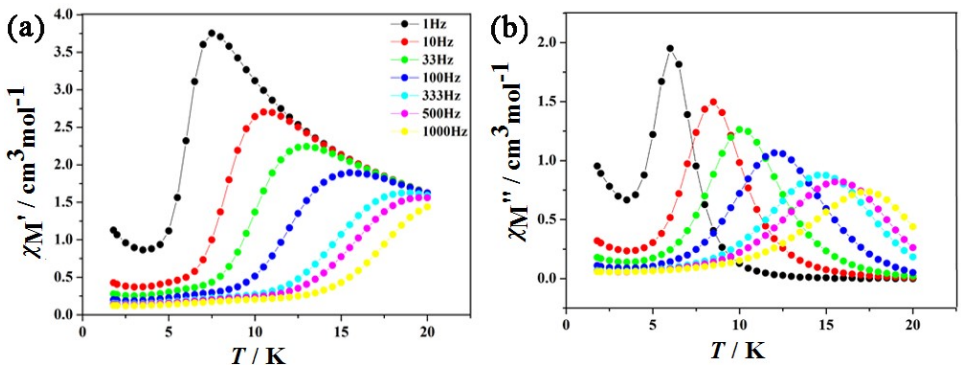

Figure S16. Temperature dependence of the in-phase (a) and out-of-phase (b) ac susceptibility of **2** under 0 Oe dc field.

Table S8. Relaxation fitting parameters from Least-Squares Fitting of $\chi(\omega)$ data of **1** under 0 Oe.

T(K)	$\Delta\chi_1$ (cm^{3}mol^{-1})	$\Delta\chi_2$ (cm^{3}mol^{-1})	α
2.0	8.32589	0.55286	0.26838
3.0	6.36581	0.40748	0.26996
4.0	5.11041	0.33781	0.26934
5.0	4.31389	0.29523	0.25942
6.0	3.74866	0.26741	0.22102
7.0	3.33305	0.22062	0.20102
8.0	3.25901	0.00856	0.31618
9.0	2.95429	0.00856	0.31618
10.0	2.33958	0.13573	0.30683
11.0	2.12825	0.10630	0.29228
12.0	1.95826	0.07669	0.29078
13.0	1.81525	0.01133	0.29635
14.0	1.68933	0.50996	0.25898
15.0	1.54574	0.85921	0.21774

Table S9. Relaxation fitting parameters from Least-Squares Fitting of $\chi(\omega)$ data of **2** under 0 Oe.

T(K)	$\Delta\chi_1$ (cm^{3}mol^{-1})	$\Delta\chi_2$ (cm^{3}mol^{-1})	α
5.0	5.10554	0.48433	0.119445
6.0	4.43833	0.32718	0.12359
7.0	4.56265	0.16554	0.21524
8.0	3.60348	0.17707	0.14716
9.0	3.17104	0.18080	0.11787
10.0	2.83244	0.17783	0.10131
11.0	2.58672	0.16928	0.09527
12.0	2.38050	0.15095	0.10173
13.0	2.18610	0.15649	0.07828
14.0	2.03290	0.12716	0.08752

15.0	1.89541	0.11873	0.07785
16.0	1.78398	0.08201	0.08201
17.0	1.70422	0.00100	0.13098
18.0	1.59683	0.00001	0.08974

8.Results of *ab initio* investigation

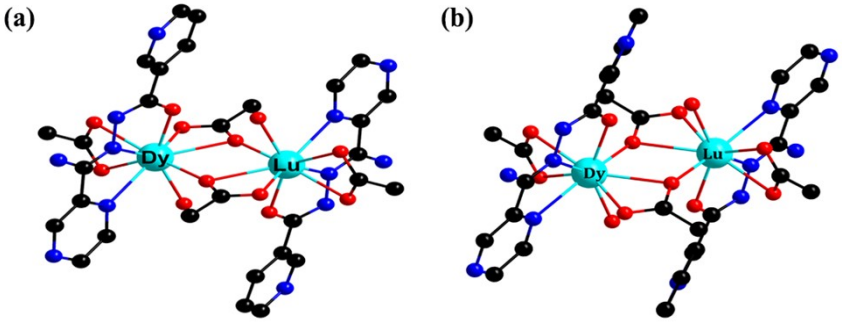

Figure S17. Calculated complete structures for compounds **1**(a) and **2**(b); H atoms are omitted.

Table S10. Calculated energy levels (cm^{-1}), g (g_x, g_y, g_z) tensors of the lowest Kramers doublets (KDs) of the Dy^{III} fragments of **1** and **2.**

1(Dy1)				**2(Dy1)**			
KDs	E/cm^{-1}	***g***		KDs	E/cm^{-1}	***g***	
1	0.0	g_x	0.012	1	0.0	g_x	0.052
		g_y	0.026			g_y	0.130
		g_z	19.610			g_z	19.500
2	114.5	g_x	0.485	2	87.3	g_x	0.272
		g_y	0.727			g_y	1.108
		g_z	16.790			g_z	17.812
3	160.8	g_x	0.051	3	124.3	g_x	0.516
		g_y	1.129			g_y	1.496
		g_z	13.153			g_z	15.383
4	186.2	g_x	1.128	4	155.4	g_x	2.875
		g_y	2.474			g_y	5.987
		g_z	14.991			g_z	10.788
5	209.6	g_x	3.349	5	192.9	g_x	1.948
		g_y	4.589			g_y	3.601
		g_z	8.054			g_z	11.122

6	279.7	g_x	2.261	6	237.5	g_x	0.700
		g_y	3.312			g_y	0.806
		g_z	10.779			g_z	17.914
7	336.8	g_x	0.690	7	310.6	g_x	0.603
		g_y	1.332			g_y	0.649
		g_z	15.102			g_z	15.849
8	447.3	g_x	0.135	8	446.1	g_x	0.081
		g_y	0.155			g_y	0.139
		g_z	19.134			g_z	18.781

Table S11. Exchange energies E (cm^{-1}) and the main values of the g_z for the lowest two exchange doublets of **1** and **2** *via* fitting the experimental $\chi_M T$ versus T (M versus H) by using POLY_ANISO program.

	Exchange doublets	**1**		**2**	
		E/cm^{-1}	g_z	E/cm^{-1}	g_z
$\chi_M T$-T	1	0.000000000000	0.000	0.000000000000	0.000
		0.000100655726		0.000011572486	
	2	0.888897492564	38.993	0.365641436088	39.218
		0.889025582364		0.365654509137	

	Exchange doublets	**1**		**2**	
		E/cm^{-1}	g_z	E/cm^{-1}	g_z
M-H	1	0.000000000000	0.000	0.000000000000	0.000
		0.000328720866		0.000005376189	
	2	0.196091489653	38.969	0.715954235118	39.209
		0.196431252064		0.715961563096	

Table S12. The angle between the *ab initio* easy axis and angle between easy axis on Dy1 and Dy1-Dy2 of compounds **1** and **2.**

Compound	Angle between two easy axis	Angle between easy axis on Dy1 and Dy1-Dy1^{i}
1	180	80.009
2	180	109.017

Table S13. The angle between the *ab initio* easy axis and the axial Dy-O/N bond of compounds **1** and **2.**

Compound	θ1 (O3)	θ2 (N2)	θ3 (O1)	θ4 (O7)	Average
1	20.602	45.318	38.957	36.046	35.231
2	31.317	33.409	55.596	6.993	31.829

Table S14. Natural Bond Order (NBO) charges per atoms in the ground state of **1** and **2** calculated within CASSCF.

1		**2**	
Dy1	2.514	Dy1	2.517
N2	−0.356	N2	−0.300
O1	−0.725	O1	−0.799
O7	−0.767	O7	**−0.782**
O3	**−0.831**	O3	−0.820
Average (axial)	**−0.670**	**Average (axial)**	**−0.675**
O4	−0.735	O4	−0.681
O5	−0.713	O5	−0.799
O6	−0.778	O6	−0.795
N1	−0.294	N1	−0.298
O2	−0.774	O2	−0.740
Average (equatorial)	**−0.659**	**Average (equatorial)**	**−0.663**
(i) 1-*x*, -*y*, 2-*z*.		(i) -*x*+1, -*y*+1, -*z*+1.	

Table S15. The results of preliminary ESP (in a.u.) analysis of **1** and **2.**

	1	**2**
ESP(equ)/ESP(ax)	**0.933305578**	**0.929298141**
ESP(ax)	-0.255712199	-0.262567533
ESP(ax_N)	-0.133373938	-0.111760563
ESP(ax_O)	-0.29649162	-0.312836522
ESP(equ)	-0.238657622	-0.24400352
ESP(equ_N)	-0.101122237	-0.09971031
ESP(equ_O)	-0.273041468	-0.280076822

Table S16. Wave functions with definite projection of the total moment | m_J > for the lowest eight KDs of individual Dy^{III} fragments for **1** and **2**.

	E/cm^{-1}	wave functions
1(Dy1)	0.0	96.5%|±15/2>
	114.5	40.6%|±13/2>+22.6%|±11/2>+11.3%|±9/2>+7.0%|±3/2>+6.2%|±5/2>
	160.8	31.1%|±13/2>+18.2%|±5/2>+16.0%|±7/2>+15.1%|±3/2>+11.9%|±1/2>
	186.2	25.6%|±9/2>+17.6%|±11/2>+13.6%|±7/2>+12.2%|±5/2>+11.5%|±1/2>+9.5%|±3/2>
	209.6	24.1%|±7/2>+16.0%|±9/2>+15.2%|±11/2>+14.0%|±1/2>+12.9%|±13/2>+9.9%|±3/2>
	279.7	26.2%|±11/2>+22.5%|±5/2>+15.3%|±3/2>+13.8%|±9/2>+10.2%|±7/2>
	336.8	23.0%|±9/2>+21.8%|±7/2>+16.3%|±5/2>+14.1%|±3/2>+11.8%|±11/2>+10.3%|±1/2>
	447.3	37.9%|±1/2>+29.1%|±3/2>+17.1%|±5/2>+8.8%|±7/2>
2(Dy1)	0.0	95.5%|±15/2>
	87.3	22.7%|±7/2>+17.6%|±5/2>+15.7%|±11/2>+14.0%|±9/2>+12.4%|±3/2>+8.6%|±1/2>
	124.3	67.6%|±13/2>+11.1%|±11/2>+10.4%|±9/2>
	155.4	23.2%|±7/2>+21.5%|±11/2>+15.2%|±9/2>+12.6%|±3/2>+11.7%|±1/2>+9.8%|±13/2>
	192.9	25.6%|±5/2>+23.7%|±3/2>+14.9%|±9/2>+11.8%|±1/2>+11.3%|±7/2>
	237.5	34.5%|±11/2>+25.1%|±9/2>+13.3%|±7/2>+10.7%|±1/2>+9.7%|±13/2>
	310.6	27.8%|±1/2>+17.3%|±3/2>+16.6%|±7/2>+15.5%|±5/2>+13.6%|±9/2>
	446.1	30.3%|±3/2>+28.0%|±1/2>+23.8%|±5/2>+12.5%|±7/2>

9.Magneto-structural correlations

Table S17. Relaxation parameters and the value of U_{eff} for nine-coordinated Dy_2 compounds with C_{4v}-CSAPR geometries.

	9/CSAPR-9/ CShM's values [a]	Bond distance/ Å		The slow relaxation process			Ref.
		Dy-Dy Intra	Dy-Dy Inter	DC field/Oe	τ_0/ s	U_{eff}/K	
[Dy_2(2,3′-ppcad)$_2$($C_2H_3O_2$)$_4$(H_2O)$_2$] (1)	**2.419**	**4.11**	**11.30**	**0**	**3.49 × 10^{-8}**	**103.43**	**In this work**
[Dy_2(2,3′-ppcad)$_2$($C_2H_3O_2$)$_4$(H_2O)$_2$]·6H_2O	**2.015**	**4.08**	**11.15**	**0**	**4.01 × 10^{-13}**	**386.48**	
[Dy_2(hfac)$_6$(H_2O)$_2$(L)] (**3**)	0.516	5.963	17.497	0	2.4 × 10^{-6}	15.4	S7
[Dy_2L(H_2L)(teaH_2)(o-vanillin)(H_2O)](ClO_4)$_2$·2CH_3OH·H_2O (**4**)	1.283 1.154	3.549	-	0	1.7× 10^{-4}	1.4	S8
[Dy_2L_2(OAc)$_4$(MeOH)$_2$]·2MeOH (**5**)	1.197	4.074	-	0	6.4 × 10^{-7}	39.1	S9
[Dy_2(Mq)$_4$(NO_3)$_6$] (**6**)	2.401	3.914	9.598	0	5.44 × 10^{-6}	40.01	S10
[Dy_2(HL_1)$_2$(NO_3)$_4$] (**7**)	2.948	3.709	7.040	No peaks	-	-	S11
[Dy_2(H_2L)$_2$(μ-piv)$_2$(piv)$_2$]·2$CHCl_3$ (**8**)	0.968	3.633	-	0 0	8.81 × 10^{-5} 1.48 × 10^{-6}	8.96 35.5	S12
[Dy_2(H_3L)$_2$(PhCOO)$_4$]·4H_2O (**9**)	1.408	3.695	> 7.6	0	1.31 × 10^{-7}	42.7	S13
[Dy_2(μ_2-anthc)$_4$(anthc)$_2$(2,2′-bpy)$_2$] (**10**)	2.300	3.949	9.318	0	3.2 × 10^{-8}	51.2	S14
[Dy_2(μ_2-anthc)$_4$(anthc)$_2$(1,10-phen)$_2$] (**11**)	1.740	3.918	9.798	0	4.6 × 10^{-9}	49.4	
[Dy_2(μ_2-anthc)$_4$(anthc)$_2$$L_2$] (**12**)	1.878	3.922	11.748	0	3.4 × 10^{-8}	31.6	
[Dy_2(ovph)$_2$$Cl_2$($H_2O$)$_3$(EtOH)] (**13**)	1.221	3.954	6.256	0	1.36 × 10^{-7}	110	S15
[Dy_2(bzhdep-2H) (NO_3)$_4$(DMF)$_4$] (**14**)	2.319	-	7.882	1000	2.6 × 10^{-6}	29.5	S16
[Dy(L_1)$_3$(DMSO)(H_2O)]$_2$ (**15**)	2.296	4.157	9.533	2000	-	-	S17
{[Dy_2(PDOA)$_3$(H_2O)$_6$]·2H_2O}$_n$ (**16**)	1.742	6.407	13.921	2000	6.3 × 10^{-10}	71.6	S18
[Dy_2(PDOA)$_3$(H_2O)$_6$]·3.5H_2O (**17**)	1.186	6.130	12.388	2000	2.4 × 10^{-11}	97.8	
[$Dy_2$$Lz_2(OAc)_6$]·2$CH_3OH$ (**18**)	1.677	3.980	-	900	3.8 × 10^{-7}	44.0	S19
Dy_2(L^1)$_2$(NO_3)$_2$(OAc)$_2$(CH_3OH)$_2$ (**19**)	2.139	4.092	-	0	1.7 × 10^{-5}	19.6	S20
{[Dy_2(β-ala)$_6$(H_2O)$_4$](ClO_4)$_6$·H_2O}$_n$ (**20**)	1.186	3.984	-	1000	4.6 × 10^{-9}	29.4	S21
[Dy_2(L^2)$_2$(NO_3)$_4$] (**21**)	5.250	-	-	0 1500	2.0 ×10^{-4} 8.56 ×10^{-4}	2.66 8.43	S22
[Dy_2(hfac)$_6$(H_2O)$_2$(Q)] (**22**)	0.178	21.656	6.071	0	7.6 × 10^{-7}	18.3	S23
[Dy_2(2,4′-pcad)$_2$($C_2H_3O_2$)$_4$(H_2O)$_2$]·4H_2O (**23**)	2.336	4.17	11.00	0	5.7 × 10^{-6}	53.5	S24
[Dy_2(2,3′-pcad)$_2$($C_2H_3O_2$)$_4$(H_2O)$_2$] (**24**)	2.167	4.13	11.39	0	3.8 × 10^{-7}	132.6	

[a] CShM's values of the Dy^{III} ion in comparison with all of the reference standard nine-coordinate polyhedrons were calculated using the SHAPE program. Abbreviation： hfac- = 1,1,1,5,5,5-hexafluoroacetylacetonate anion ; L = 4,4′,7,7′-tetra-tert-butyl-2,2′-bi-1,3-benzodithiole-5,5′,6,6′-tetrone ; teaH_3 = triethanolamine ; HL= *N*,*N*-bis(3-methoxysalicylidene)-1,2-cyclohexanediamine ; HL = (E)-*N*'-(2-hydroxybenzylidene)-2-mercaptonicotinohydrazide; Mq = 8-hydroxy-2-methylquinoline ; H_2L_1 = 2-[(2-hydroxy-ethyl)-pyridin-2-ylmethylamino]-ethanol ; H_3L = 2,2'-(2-hydroxy-3-methoxy-5-methylbenzylazanediyl)diethanol ; H_4L = 1,5-Bis(2-hydroxy-3-methoxybenzylidene)carbonohydrazide ; anthc− = 9-anthracenecarboxylate ; HL = 2,2'-bipyridyl, 1,10-phenanthroline, and 4,7-dimethyl-1,10-phenanthroline ; H_2ovph = pyridine-2-carboxylic acid [(2-hydroxy-3-methoxyphenyl)methylene] hydrazide ; bzhdep = Pyrazine-2,

5-diylbis(ethan-1-yl-1-ylidene)di(benzohydrazide) ; HL1= 2-methoxycinnamic acid ; H_2PDOA = 1,2-phenylenedioxydiacetic acid ; Lz = 6-pyridin-2-yl-[1,3,5]triazine-2,4-diamine ; HL1= ((E)-1-(((1-methyl-1H-benzo[d]imidazol-2-yl)methylene)amino)naphthalen-2-ol) ; β-ala = β-alanine ; HL_2 = 2-(pyridin-2-yl)hexahydropyrimidin-5-ol ; hfac = 1,1,1,5,5,5-hexafluoroacethylacetonate ; Q = 2,2'-cyclohexa-2,5-diene-1,4-diylidenebis(4,7-di-tert-butyl-1,3-benzodithiole-5,6-dione) ; 2,4'-Hpcad = N^3-(2-pyridoyl)-4-pyridinecarboxamidrazone ; 2,3'-Hpcad =N^3-(2-pyridoyl)-3-pyridinecarboxamidrazone.

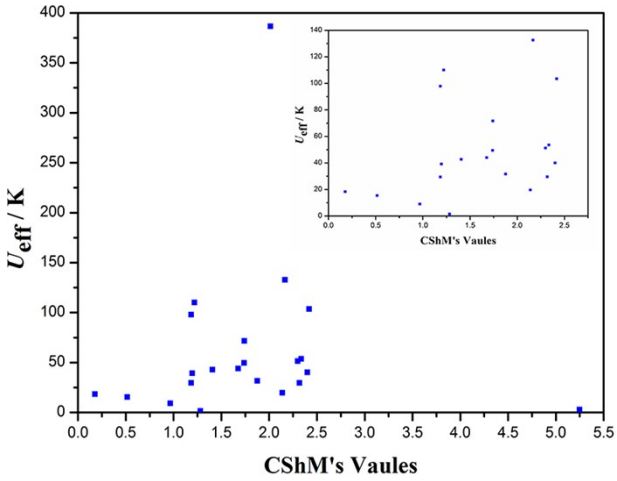

Figure S18. The relationship between coordination configuration and SMMs behavior.

References

[S1] M. E. Lines, *J. Chem. Phys.,* 1971, **55**, 2977-2984.

[S2] K. C. Mondal, A. Sundt, Y. H. Lan, G. E. Kostakis, O. Waldmann, L. Ungur, L. F. Chibotaru, C. E. Anson and A. K. Powell, *Angew. Chem. Int. Ed.*, 2012, **51**, 7550.

[S3] S. K. Langley, D. P. Wielechowski, V. Vieru, N. F. Chilton, B. Moubaraki, B. F. Abrahams, L. F. Chibotaru and K. S. Murray, *Angew. Chem. Int. Ed.*, 2013, **52**, 12014.

[S4] L. F. Chibotaru, L. Ungur, and A. Soncini, *Angew. Chem. Int. Ed.*, 2008, **47**, 4126.

[S5] L. Ungur, W. Van den Heuvel and L.F. Chibotaru, *New J. Chem.*, 2009, **33**, 1224.

[S6] L. F. Chibotaru, L. Ungur, C. Aronica, H. Elmoll, G. Pilet and D. Luneau, *J. Am. Chem. Soc.*, 2008, **130**, 12445.

[S7] F. Pointillart, S. Klementieva, V. Kuropatov, Y. Le Gal, S. Golhen, O. Cador, V. Cherkasov and L. Ouahab, *Chem. Commun.,* 2012, **48**, 714-716.

[S8] L. Zhang, P. Zhang, L. Zhao, S. Y. Lin, S. F. Xue, J. K. Tang and Z. L. Liu, *Eur. J. Inorg. Chem.,* 2013, **8**, 1351-1357.

[S9] H. Zhang, S. Y. Lin, S. Xue, C. Wang and J. K. Tang, *Dalton Trans.,* 2014, **43**, 6262-6268.

[S10] F.Yang, Q. Zhou, G. Zeng, G. H. Li, L. Gao, Z. Shi and S. H. Feng, *Dalton Trans.,* 2014, **43**, 1238-1245.

[S11] Y.Peng, V. Mereacre, A. Baniodeh, Y. Lan, M. Schlageter, G. E. Kostakis and A. K. Powell, *Inorg. Chem.,* 2016, **55**, 68-74.

[S12] P. Bag, C. K. Rastogi, S. Biswas, S. Sivakumar, V. Mereacre and V. Chandrasekhar, *Dalton Trans.,* 2015, **44**, 4328-4340.

[S13] H. S. Ke, S. Zhang, X. Li, Q. Wei, G. Xie, W. Y. Wang and S. P. Chen, *Dalton Trans.,* 2015, **44**, 21025-21031.

[S14] Y. L. Wang, C. B. Han, Y. Q. Zhang, Q. Y. Liu, C. M. Liu and S. G. Yin, *Inorg. Chem.,* 2016, **55**, 5578-5584.

[S15] Y. Jiang, G. Brunet, R. J. Holmberg, F. Habib, I. Korobkov and M. Murugesu, *Dalton Trans.,* 2016, **45**, 16709-16715.

[S16] W. Huang, F. X. Shen, S. Q. Wu, L. Liu, D. Wu, Z. Zheng, J. Xu, M. Zhang, X. C. Huang, J. Jiang, F. Pan, Y. Li, K. Zhu and O. Sato, *Inorg. Chem.,* 2016, **55**, 5476-5484.

[S17] O. Khalfaoui, A. Beghidja, J. Long, A. Boussadia, C. Beghidja, Y. Guari and J. Larionova, *Dalton Trans.,* 2017, **46**, 3943-3952.

[S18] R. Boca, M. Stolarova, L. R. Falvello, M. Tomas, J. Titis and J. Cernak, *Dalton Trans.,* 2017, **46**, 5344-5351.

[S19] M. Guo, Y. H. Xu, J. F. Wu, L. Zhao and J. K. Tang, *Dalton Trans.,* 2017, **46**, 8252-8258.

[S20] H. L.Wang, J. M. Peng, Z. H. Zhu, K. Q. Mo, X. F. Ma, B. Li, H. H. Zou and F. P. Liang, *Cryst. Growth Des*., 2019, **19**, 5369-5375.

[S21] M. Orts-Arroyo, I. Castro, F. Lloret and J. Martinez-Lillo, *Dalton Trans*., 2020, **49**, 9155-9163.

[S22] Z. H. Zhu,H. L. Wang, S. Yu, X. X. Fu, H. H. Zou, Z. Chen and F. P. Liang, *Appl. Organometal Chem.,* 2020, **34**, e5622.

[S23] F. Pointillart, J. Flores Gonzalez, V. Montigaud, L. Tesi, V. Cherkasov, B. Le Guennic, O. Cador, L. Ouahab, R. Sessoli and V. Kuropatov, *Inorg. Chem. Front.,* 2020, **7**, 2322-2334.

[S24] L. Sun, S. L. Wei, J. Zhang, W. Y. Wang, S. P. Chen, Y. Q. Zhang, Q. Wei, G. Xie, and S. L. Gao, *J. Mater. Chem. C,* 2017, **5**, 9488-9495.